(2)

NASA
Technical Memorandum 102513

AVSCOM
Technical Report 90-C-006

The Effect of Coatings and Liners on Heat Transfer in a Dry Shaft-Bush Tribosystem

Mihir K. Ghosh
Lewis Research Center
Cleveland, Ohio

and

David E. Brewe
Propulsion Directorate
U.S. Army Aviation Systems Command
Lewis Research Center
Cleveland, Ohio

August 1990

NASA

US ARMY
AVIATION
SYSTEMS COMMAND
AVIATION R&T ACTIVITY

THE EFFECT OF COATINGS AND LINERS ON HEAT TRANSFER IN A DRY SHAFT-BUSH TRIBOSYSTEM

Mihir K. Ghosh*
National Aeronautics and Space Administration
Lewis Research Center
Cleveland, Ohio 44135

and

David E. Brewe
Propulsion Directorate
U.S. Army Aviation Systems Command
NASA Lewis Research Center
Cleveland, Ohio 44135

Summary

The temperatures due to frictional heating within a solid lubricated or coated journal bearing were analyzed by using a finite element method. A solid model of the shaft-bush tribocontact was generated with an eight-node, three-dimensional, first-order isoparametric heat-transfer element and the Patran solid modeler software. The Patmar (Patran-Marc) translator was used to help develop the Marc-based finite element program for the system; this software was used on the Cray X-MP super computer to perform a finite element analysis of the contact. The analysis was performed for various liner materials, for thin, hard, wear-resistant coated bearings, and for different geometries and thermal cooling boundary conditions. The analyses indicated that thermal conductivity of the liner or coating material is the most vital thermal parameter that controls the interface temperature. In addition to design variations, the proximity of the cooling source to the heat-flux-generating interface is critically important to the temperature control in the system.

Introduction

The temperature rise due to frictional heating at the interface of tribocontacts has attracted the attention of engineers and tribologists in recent years. Friction and wear of dry contacts are dependent on the overall temperature increase at the interface. Thermomechanical effects, such as the initiation of thermal cracks and the low-cycle thermal-fatigue failure in dry bearings and seals, are dependent on the heat dissipation mechanism and the overall temperature rise. Floquet, Play, and Godet (ref. 1) used a two-dimensional Fourier transform method developed by Ling (ref. 2) to calculate the contact temperatures in dry bearings operating with a plastic liner. Later, Floquet and Play extended this technique to three-dimensional problems (ref. 3). They showed that small changes in the design may bring large differences in contact temperatures, and that to reduce the maximum temperature, the rubbing surfaces must be as close as possible to a controlled temperature heat sink and must not be shielded by any thermal barrier. Gecim and Winer (refs. 4 and 5) extended the Fourier transform method to calculate steady temperatures in a rotating cylinder that had multiple surface heat sources and a variety of geometries and thermal boundary conditions.

In recent years, high-temperature applications brought about the need for hard, wear-resistant coatings (viz., Al_2O_3, and ZrO_2) to be used as thermal barriers in mechanical components. When these components are subjected to heavily loaded sliding conditions, "heat checking" often occurs; that is, cracking in the neighborhood of the contact zone due to the combination of thermal heating and mechanical load. This often occurs in such mechanical devices as seals and brakes. Kennedy, et al. (refs. 6 to 8) have done thermomechanical analyses of dry sliding contacts, using a finite element

*National Research Council – NASA Research Associate at Lewis Research Center, on leave from Mechanical Engineering Dept., I.T., B.H.U., Varnasi, 221005, India.

technique. In particular, a recent investigation (ref. 8) addressed the problems of hard, wear-resistant coatings on a ductile metallic substrate, as applied to mechanical face seals. A thermo-elasto-plastic analysis of stresses and deformations was used.

Ju and Chen (ref. 9) used a Fourier transform method to investigate the mechanical stresses, temperature field, and thermal stresses due to a moving frictional load. Ju and Liu (refs. 10 and 11) extended this technique to study the phenomenon of thermomechanical cracking in layered media. Leroy, Floquet, and Villechaise (ref. 12) also used a fast Fourier transform algorithm to study thermomechanical behavior of layered media.

Fourier transform techniques generally provide useful analytical expressions, but they are limited in applications dealing with irregular geometries and boundaries. Insofar as we know, dry bearing temperatures have not been investigated with the finite element technique that accommodates irregular boundaries. Herein, results of a finite element analysis of dry contact temperatures due to frictional heating at the interface of a shaft-bush-housing system are presented. A solid model of the system was generated with the Patran solid modeler software, and the finite element analysis was done with the Marc finite element software. The temperature distribution in the system was determined with various liner materials, coating materials, coating thicknesses, and bearing geometries.

This work also shows that the method can serve as a computer-aided design technique to model mechanical components (such as the cylinder-piston of an advanced low heat rejection (LHR) diesel engine or Stirling engine, and aircraft control and undercarriage bearings) for temperature rise and thermal distortions under specific operating conditions.

Symbols

$[\mathbf{B}]$	temperature gradient interpolation matrix
$[\mathbf{C}]$	capacitance matrix
c	specific heat, J/kg °C
f	friction coefficient at the contact
h	film heat transfer coefficient, W/m^2 °C
$[\mathbf{K}]$	heat transfer or coefficient matrix
k	thermal conductivity, W/m °C
M	number of finite elements
$[\mathbf{N}]$	temperature interpolation matrix
$\hat{\mathbf{n}}$	unit vector
p	contact pressure, Pa
Q	internal heat generation
q	heat flux distribution, W/m^2 or N/cm-sec
$\mathbf{R}$	heat load matrix
R_{in}	inner radius of the bearing, m
r	number of nodes in an element
S	surface area, m^2
T	temperature, °C
t	time, sec
V	rubbing velocity, m/sec
x,y,z	Cartesian coordinates
Γ	surface of integration, m^2
κ	thermal diffusivity, m^2/sec
ρ	density, kg/m^3
Ω	volume of integration, m^3
ω_s	angular speed of the shaft, rad/sec

Subscripts:

c	conductance
e	element, in a global sense
h	surface convection
m	maximum
q	surface heating
s	surface
T	nodal temperatures

Superscript:

e	element, in a local sense

Theory

The theory discussed herein is taken from reference 13.

Finite Element Formulation

The steady-state or transient heat transfer in a three-dimensional anisotropic solid moving with velocity V is governed by the Fourier heat conduction or energy equation, which is written as

$$\nabla \cdot k \nabla T - \rho c \left[\left(\frac{\partial T}{\partial t} \right) - V \cdot \nabla T \right] + \dot{Q} = 0 \qquad (1)$$

where $\dot{Q}(x,y,z,t)$ is the internal heat generation rate per unit volume. The solution for the temperature distribution must satisfy the boundary conditions and initial conditions on all portions of the surface. The inertia conditions, which specify the temperature at time zero, are required for the transient analysis. The heat conduction boundary conditions are as follows:

$$\left.\begin{aligned} T &= T_1 \\ q\cdot\hat{\mathbf{n}} &= -\kappa\,\nabla T\cdot\hat{\mathbf{n}} \\ h(T_s - T_e)\cdot\hat{\mathbf{n}} &= k\,\nabla T\cdot\hat{\mathbf{n}} \end{aligned}\right\} \quad (2)$$

where

T_1 prescribed temperature in the specified region S_1 of the surface

$-\kappa\,\nabla T\cdot\hat{\mathbf{n}}$ prescribed heat flux normal to the surface S_2

$k\,\nabla T\cdot\hat{\mathbf{n}}$ convection to exchange temperature T_e from the surface with unknown temperature T_s

The solution domain in the solid is discretized into M finite elements possessing r nodes. Temperature and temperature gradients within the element are expressed in terms of nodal temperatures as

$$T^e(x,y,z,t) = [\mathbf{N}(x,y,z,t)]\ T(t)$$

and

$$\left\{\begin{matrix} \dfrac{\partial T}{\partial t}(x,y,z,t) \\ \dfrac{\partial T}{\partial t}(x,y,z,t) \\ \dfrac{\partial T}{\partial t}(x,y,z,t) \end{matrix}\right\} = [\mathbf{B}(x,y,z)]\ T(t) \quad (3)$$

where [N] is the temperature interpolation matrix, and [B] is the temperature gradient interpolation matrix such that,

$$[\mathbf{N}(x,y,z)] = [\mathbf{N}_1, \mathbf{N}_2, \ldots, \mathbf{N}_r]$$

and

$$[\mathbf{B}(x,y,z)] = \begin{bmatrix} \dfrac{\partial \mathbf{N}_1}{\partial x} & \dfrac{\partial \mathbf{N}_2}{\partial x} & \cdots & \dfrac{\partial \mathbf{N}_r}{\partial x} \\ \dfrac{\partial \mathbf{N}_1}{\partial y} & \dfrac{\partial \mathbf{N}_2}{\partial y} & \cdots & \dfrac{\partial \mathbf{N}_r}{\partial y} \\ \dfrac{\partial \mathbf{N}_1}{\partial z} & \dfrac{\partial \mathbf{N}_2}{\partial z} & \cdots & \dfrac{\partial \mathbf{N}_r}{\partial z} \end{bmatrix} \quad (4)$$

Finite element equations are derived from the energy equation (eq. 1) by using the method of weighted residuals (Galerkin's method):

$$[\mathbf{C}]\left\{\frac{\partial T}{\partial x}\right\} + [[\mathbf{K}_c] + [\mathbf{K}_h]]\ \{T\} = \mathbf{R}_Q + \mathbf{R}_q + \mathbf{R}_h + \mathbf{R}_T \quad (5)$$

where

$$\left.\begin{aligned} [\mathbf{C}] &= \int_{\Omega^e} \rho c\,\mathbf{N}\ [\mathbf{N}]\,d\Omega \\ [\mathbf{K}_C] &= \int_{\Omega_e} [\mathbf{B}]^T[\mathbf{K}][\mathbf{B}]d\Omega \\ [\mathbf{K}_h] &= \int_{s_3} h\,\mathbf{N}\,[\mathbf{N}]d\Gamma \\ \mathbf{R}_Q &= \int_{\Omega} Q\,\mathbf{N}\,d\Omega \\ \mathbf{R}_q &= \int_{s_2} q_s\,\mathbf{N}\,d\Gamma \\ \mathbf{R}_h &= \int_{s_3} hT_e\,\mathbf{N}\,d\Gamma \\ \mathbf{R}_T &= -\int_{s} (q\cdot\hat{\mathbf{n}})\ \mathbf{N}\,d\Gamma \end{aligned}\right\} \quad (6)$$

The coefficient matrix [C] of the time derivative of the nodal temperatures is the element capacitance matrix. The coefficient matrices $[\mathbf{K}_c]$ and $[\mathbf{K}_h]$ are element conductance matrices and relate to conductance and convection.

The vectors $\mathbf{R}_T$, $\mathbf{R}_Q$, $\mathbf{R}_q$, $\mathbf{R}_h$ are heat-load vectors arising from specified nodal temperatures, internal heat generation, specified surface heating, and surface convection, respectively. For steady-state analysis, equation (5) reduces to

$$[[\mathbf{K}_C] + [\mathbf{K}_h]]\ T = \mathbf{R}_Q + \mathbf{R}_q + \mathbf{R}_h \quad (7)$$

Problem Statement and Solution Methodology

In the present work a shaft-bush/liner-housing type of tribosystem was analyzed. The system, shown in figure 1, consists of a hollow shaft (1) rotating in a bush-liner (2) fitted within a stationary housing (3). Alternatively, the shaft rotates in a housing with a thin, hard, wear-resistant ceramic coating at its internal surface. There is frictional rubbing at the interface of the liner or coating and the shaft. Frictional heating at the interface is conducted to the shaft and the bearing and housing, thereby causing a temperature rise in both. The main objective of the present study was to develop a finite element model of the previously described system by using the Patran solid modeler software, and thereafter to obtain a Marc finite element program by using a Patran-Marc (Patmar) translator. Following this, we analyzed the problem for temperature distribution within the solid, using the Marc finite element software, subject to the proper boundary conditions and the appropriate material thermal properties. The results were

postprocessed with the Patran postprocessor. The boundary conditions for the system analyzed were

(1) A heat-transfer coefficient h equal to 58 W/m^2 °C and a reference temperature of 20 °C, caused by natural convection
(2) An imposed temperature of 35 °C at the outer ends of the shaft, because of direct cooling
(3) An imposed temperature of 35 °C at the periphery of the housing, because of direct cooling
(4) An imposed temperature of 35 °C for Case I, caused by direct cooling at the inner radius of the shaft

Shaft speeds of 2.6, 6.5, and 13.0 rad/sec were used to calculate the heat flux generated at the interface. A nodal heat flux q equal to the product of the contact pressure p, the friction coefficient f, and the rubbing velocity V was input to the interface between the shaft and bush (or coated) housing. An harmonic contact pressure distribution extending from $\pm 90°$ was assumed (i.e., the journal contacts of half the bearing).

Effects of various liner materials, coating materials, coating thicknesses, and geometries on the temperature distribution and the maximum temperature at the interface were investigated.

Results and Discussion

The maximum interface temperatures and the temperature distribution in the shaft-bearing system are presented herein. This system was composed of either a bearing with liner material in a housing, or a bearing with a thin, hard, wear-resistant coating on its inner surface. The temperature rise was due to frictional heating at the interface. The hollow shaft had different dimensions (see table I) for the three cases studied: (1) bearings with soft liner materials; (2) bearings with thin, hard coatings on the internal surface; and (3) variations in geometry (table II) and the cooling condition. Nodal heat flux generated in the contact was estimated to be equal to the product of the contact pressure, rubbing velocity, and friction coefficient. The coefficients of friction for the liner and coating materials ranged from 0.15 to 0.3. However, an intermediate value of 0.2 was assumed. Our objective was to evaluate the temperature rise in the contact for the same amount of heat flux input. A harmonic pressure distribution extending from $\pm 90°$ was assumed.

Thus, heat flux distribution

$$q = q_m \cos \phi$$

where

$$q_m = fVp_m$$

and

f friction coefficient at the contact, assumed to be 0.2

V rubbing velocity; $R_{h_i}\omega_s$

p_m maximum contact pressure

Case I—Bearings with Soft Liner Materials

Thermal properties of various liner materials are shown in table III. The shaft and the housing were made of steel. For a 6.0-mm thick liner, the maximum interface temperatures obtained for various liner materials are shown in table IV. The lowest of the maximum temperatures was 108.5 °C for the graphitized metal liner, which had the highest thermal conductivity and diffusivity values. As the material's conductivity and diffusivity decreased, the temperature at the interface increased. In the absence of convection, the thermal conductivity of the liner was the material's single most important thermal property, influencing both the temperature rise at the interface and the temperature distribution as well (fig. 2). Table V shows the variation of maximum interface temperature with five different heat distribution functions for a resin liner material (ref. 1), while keeping all other conditions constant. We observed that the maximum interface temperature and the temperature distribution can differ significantly with the nature of the heat distribution in the contact region (fig. 3). The nature of the heat distribution depends on the contact pressure in the contact region, which in turn depends on the geometry and the type of loading. The nature of the loading may vary with the operating conditions.

The effects of the magnitude of the load and the thickness of the liner material are shown in table VI. Not surprisingly, a thicker liner material can result in a lower interface temperature, provided the conductivity of the liner material is higher than the conductivity of the bush material. Thus, for higher loads or pV factors, a thicker graphitized metal liner would help reduce the temperatures.

Case II—Bearings with a Thin, Hard Coating on the Internal Surface

Thermal properties of thin, hard, coating materials are given in table VII. For a 1.0-mm-thick coating, the variations in maximum interface temperatures are shown in table VIII. As is evident from table VII for the thermal properties and table VIII for the maximum temperatures, the thermal conductivity of the coating material determines the magnitude of the maximum interface temperature. When a coating material with low thermal conductivity was used as a thermal barrier to shield the bearing, high temperatures occurred at the shaft-bearing interface, thereby dissipating more heat to the shaft and causing higher shaft temperatures.

In order to study the effect of coating thickness, calculations were made for titanium nitride coatings ranging from 0.125 to 1.0 mm thick. The resulting maximum interface temperatures are shown in table IX. Note that maximum interface temperatures decreased with decreasing coating thickness. This means that thicker coatings with lower conductivity than the substrate (such as titanium nitride on steel) are better thermal barriers than very thin coatings. Temperature distributions in the system, which result from using three different thicknesses of titanium nitride coating,

are shown in figures 4 to 6. Similar calculations for various thicknesses of tungsten carbide coatings showed almost no change in maximum interface temperature, since tungsten carbide has a higher thermal conductivity than the steel substrate.

Case III—Variations in Geometry and the Cooling Condition

Tables X and XI show the variation of maximum interface temperatures for a number of bearing outer radii and bearing lengths. Other dimensions remained the same. Higher interface temperatures occurred with larger bearing diameters, since the cooling source was located at the outer bearing diameter. An increase in bearing length did not alter the maximum temperature. For a hollow shaft that was cooled internally, the interface temperature was drastically reduced—from 203 to 109 °C. The thermal properties of the materials are considered to be temperature-independent here. Figures 7 to 10 show the changes in the temperature distribution in the system because of geometry variation and inner surface cooling of the hollow shaft.

An increase in rubbing velocity or pV factor can cause a tremendous rise in the maximum interface temperatures. Table XII shows that temperatures as high as 928.0 °C can be obtained at $pV = 5362.5$ N/cm-sec with a 1.0-mm thick titanium nitride coating. Figure 11 illustrates the thermal distribution for this case.

Summary of Results

A Patran solid modeling package was used to generate a finite element model for the thermal analysis of a shaft-bush tribosystem. The Marc finite element software was used to determine the temperature distribution in the tribosystem. These software permit finite element modeling of bearings and seals so that temperature distributions can be calculated in specific applications. Mechanical components (viz., the cylinder-piston of an advanced LHR diesel engine, the Stirling cycle engine for space power applications, aircraft control and undercarriage bearings, and so on) can be modeled for temperature-rise and thermal distortions under specific operating conditions. The results of our analysis can be summarized as follows:

1. If a constant friction coefficient is assumed, thermal conductivity of the liner or coating material is the most important thermal property for controlling temperatures in tribocontacts.
2. Design changes in bearing diameter and length can result in significant differences in the interface temperature.
3. Interface temperatures can be substantially reduced by cooling the inner surface of the hollow shaft.
4. Designs that can provide a cooling medium in close proximity to the heat-flux-generating interface would be most effective in reducing the temperature rise in the contact.

References

1. Floquet, A.; Play, D.; and Godet, M.: Surface Temperature in Distributed Contacts: Application to Bearing Design. J. Lubr. Technol., vol. 99, no. 2, Apr. 1977, pp. 277-283.
2. Ling, F.F.: Surface Mechanics. Wiley, 1973.
3. Floquet, A.; and Play, D.: Contact Temperature in Dry Bearings: Three Dimensional Theory and Verification. J. Lubr. Technol., vol. 103, no. 2, Apr. 1981, pp. 243-252.
4. Gecim, B.; and Winer, W.O.: Steady Temperature in a Rotating Cylinder Subject to Surface Heating and Convective Cooling. J. Tribol., vol. 106, no. 1, Jan. 1984, pp. 120-127.
5. Gecim, B.; and Winer, W.O.: Steady Temperatures in a Rotating Cylinder—Some Variations in the Geometry and the Thermal Boundary Conditions. J. Tribology, vol. 108, no. 3, July 1986, pp. 46-454.
6. Kennedy, F.E., Jr.: Surface Temperatures in Sliding Systems—A Finite Element Analysis. J. Lubr. Technol., vol. 103, no. 1, Jan. 1981, pp. 90-96.
7. Kennedy, F.E., et al.: Improved Techniques for Finite-Element Analysis of Sliding Surface Temperatures. Developments in Numerical and Experimental Methods Applied to Tribology, D. Dowson, et al., eds., Butterworths, 1984, pp. 138-150.
8. Kennedy, F.E.; and Hussaini, S.Z.: Thermo-Mechanical Analysis of Dry Sliding Systems. Comput. Struct., vol. 26, no. 1/2, 1987, pp. 345-355.
9. Ju, F.D.; and Chen, T.Y.: Thermomechanical Cracking in Layered Media from Moving Friction Load. J. Tribology, vol. 106, no. 4, Oct. 1984, pp. 513-518.
10. Ju, F.D.; and Liu, J.C.: Parameters Affecting Thermo-Mechanical Cracking in Coated Media Due to High-Speed Friction Load. J. Tribology, vol. 110, no. 2, Apr. 1988, pp. 222-227.
11. Ju, F.D.; and Liu, J.C.: Effect of Peclet Number in Thermo-Mechanical Cracking Due to High-Speed Friction Load. J. Tribology, vol. 110, no. 2, Apr. 1988, pp. 217-221.
12. Leroy, J.M.; Floquet, A.; and Villechaise, B.: Thermochemical Behavior of Multilayered Media: Theory. J. Tribology, vol. 111, no. 3, July 1989, pp. 538-544.
13. Huebner, K.H.; and Thornton, E.A.: The Finite Element Method for Engineers. 2nd ed., Wiley, 1982.
14. Malik, R.A.; and Freeman, P.: Development of a Modified PV—Criterion for Dry Bearings. ASLE International Conference on Solid Lubrication, ASLE, 1971, pp. 143-156.

TABLE I.—SHAFT SPECIFICATION AND BEARING DIMENSIONS FOR THREE CASES

Case	Shaft			Bearing		
	Outer radius, cm	Inner radius, cm	Length, cm	Outer radius, cm	Inner radius, cm	Length, cm
[a]I and [a]II	2.5	1.5	8.4	6.0	2.5	1.2
[b]III	2.5	1.5	16.0	5.0	2.5	1.6

[a]Bearing is set off shaft to right by 1.2 cm.

[b]Bearing is centrally located on shaft.

TABLE II.—GEOMETRY VARIATIONS FOR CASE III

Bearing length, cm	Bearing outer radius, cm
1.6	3.2
1.6	5.0
1.6	8.0
3.2	5.0

TABLE III.—THERMAL PROPERTIES OF LINER MATERIALS

[From ref. 14.]

Liner Material	Specific heat, c, J/kg °C	Thermal conductivity, k, W/m °C	Density, ρ, kg/m^3	Diffusivity, $\kappa/\rho c$, m^2/sec
Graphitized metal	377.0	127.4	7039.0	4.8×10^{-5}
PTFE-bronze	394.0	42.5	6501.6	1.66×10^{-5}
Carbon graphite	754.0	3.35	2101.7	2.1×10^{-6}
PTFE-thermoset	942.8	.263	2293.2	1.1×10^{-6}
PTFE-ceramic	838.0	.337	2376.0	1.69×10^{-7}
Mo_2S-nylon	188.6	.25	1198.0	1.22×10^{-7}
Resin	1214.0	.233	1200.0	1.6×10^{-7}

TABLE IV.—MAXIMUM INTERFACE TEMPERATURES FOR VARIOUS LINER MATERIALS

[Heat flux distribution $q = q_m \cos\phi$; pV = 1072.5 N/cm-sec; liner thickness = 6.0 mm.]

Liner material	Maximum temperature, °C
Graphitized metal	108.5
PTFE-bronze	118.6
Carbon graphite	147.0
PTFE-thermoset	152.8
PTFE-ceramic	152.7
Mo_2S-nylon	152.8
Resin	152.8

TABLE V.—MAXIMUM INTERFACE TEMPERATURES FOR VARIOUS HEAT FLUX DISTRIBUTION FUNCTIONS

[Resin liner thickness = 6.0 mm; pV = 1072.5 N/cm-sec.]

Heat flux distribution, q, N/cm-sec	Maximum temperature, °C	Maximum temperature location, deg
$q_m\cos\phi$	152.8	0
$q_m \cdot (4/\pi)\cos^2\phi$	179.7	0
$q_m \cdot (2/\pi)(1+\sin\phi)$	169.7	±90
$q_m \cdot (2/\pi)$	114.0	0
$q_m \cdot (2/\pi)(1-\sin\phi)$	99.6	0

TABLE VI.—MAXIMUM INTERFACE TEMPERATURES FOR pV FACTORS AND LINER THICKNESSES

[Heat flux distribution $q = q_m \cos\phi$.]

(a) Resin liner, 6.0 mm thick

p_mV factor, N/cm-sec	Temperature, °C
1072.50	152.8
536.25	93.9
107.25	46.8

(b) Graphitized metal liner; pV = 1072.5 N/cm-sec

Liner thickness, mm	Temperature, °C
6.0	108.5
12.0	103.5
18.0	99.8

TABLE VII.–THERMAL PROPERTIES OF COATING MATERIALS AND SUBSTRATE

Material	Specific heat, c, J/kg °C	Thermal conductivity, k, W/m °C	Density, ρ, kg/m^3	Diffusivity $\kappa/\rho c$, m^2/sec
Aluminum	869.8	267.7	2 699.0	1.136×10^{-5}
Zirconium	17 769.0	131.9	6 513.0	1.142×10^{-6}
Silicon carbide	711.0	104.4	2 997.0	4.9×10^{-5}
Tungsten carbide	100.0	100.0	15 800.0	5.0×10^{-6}
Aluminum oxide	1 039.0	20.73	3 997.0	4.99×10^{-6}
Stellite	421.9	9.7	8 300.0	2.77×10^{-6}
Titanium nitride	590.0	4.0	5 200.0	1.3×10^{-6}
Zirconia[a]	400.0	1.8	5 750.0	7.8×10^{-5}
Steel	460.0	46.0	7 800.0	1.28×10^{-5}

[a]Partially stabilized.

TABLE VIII.—MAXIMUM INTERFACE TEMPERATURES FOR COATING MATERIALS

[Coating thickness = 1.0 mm; heat flux distribution $q = q_m\cos\phi$; pV = 1072.5 N/cm-sec.]

Coating material	Maximum temperature, °C
Aluminum	176.8
Zirconium	181.1
Silicon carbide	182.2
Tungsten carbide	182.4
Aluminum oxide	191.3
Stellite	199.5
Titanium nitride	213.0
Zirconia[a]	234.7

[a]Partially stabilized

TABLE IX.—MAXIMUM INTERFACE TEMPERATURES FOR VARIOUS TITANIUM NITRIDE COATING THICKNESSES

[Heat flux distribution $q = q_m\cos\phi$; pV = 1072.5 N/cm-sec.]

Coating thickness, mm	Maximum temperature, °C
1.0	213.0
.75	208.0
.5	201.0
.25	194.0
.125	190.0

TABLE X.—MAXIMUM INTERFACE TEMPERATURES FOR VARIOUS BEARING DIMENSIONS

[Coating, 1-mm-thick TiN; heat flux distribution $q = q_m\cos\phi$; pV = 1072.5 N/cm-sec.]

Bearing and housing outer radius, cm	Maximum temperature, °C
3.8	182.0
5.0	202.1
8.0	228.1

TABLE XI.—MAXIMUM INTERFACE TEMPERATURES FOR VARIOUS BEARING LENGTHS AND COOLING CONDITIONS

[Coating, 1-mm-thick TiN; pV = 1072.5 N/cm-sec; bearing outer radius, 5 cm.]

Bearing length, cm	Maximum temperature, °C
1.6	202.1
3.2	202.5
[a]3.2	109.0

[a]With shaft inner surface cooling.

TABLE XII.—MAXIMUM INTERFACE TEMPERATURES FOR VARIOUS pV FACTORS

[Coating, 1-mm-thick TiN; heat flux distribution $q = q_m\cos\phi$.]

pV factor, N/cm-sec	Maximum temperature, °C
1072.5	213.0
2681.25	481.7
5362.5	928.0

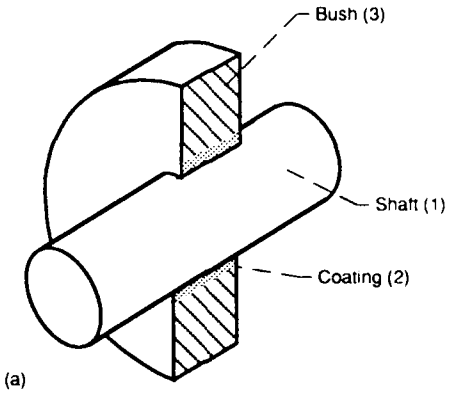

(a)

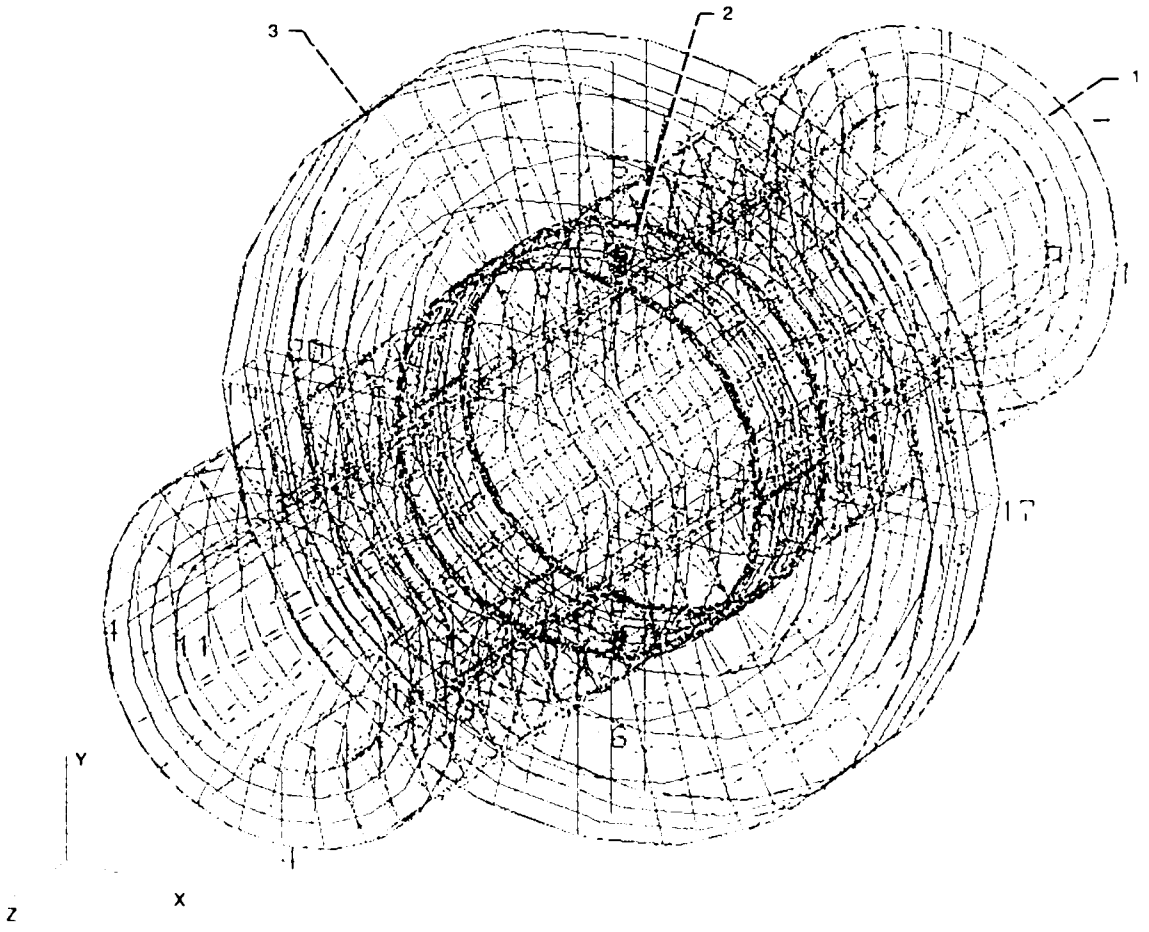

(b)

(a) Section view.
(b) Finite element model.

Figure 1 — Shaft-bush bearing tribosystem.

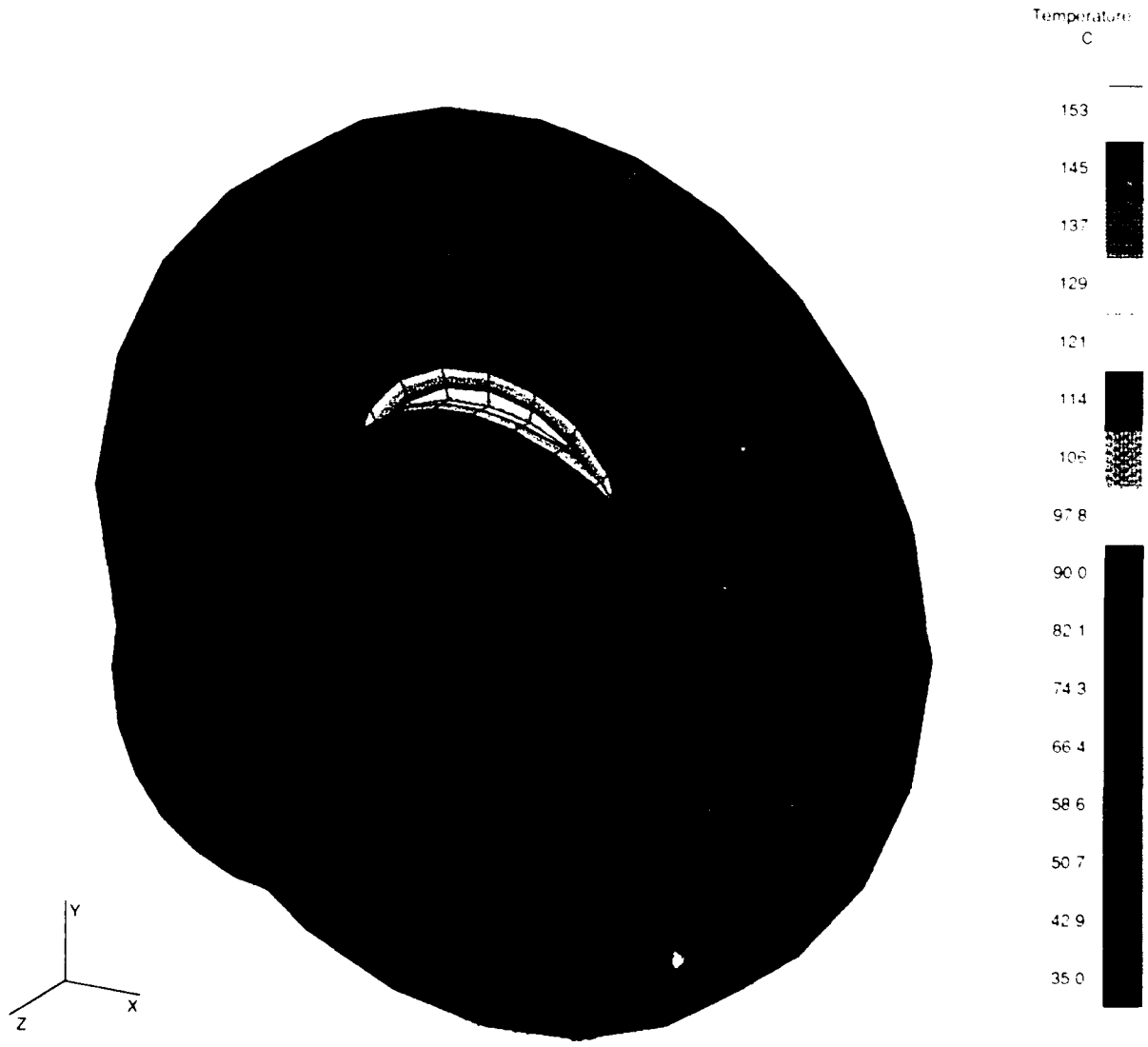

Figure 2. Tribosystem temperature contours for case I. Bearing has 6.0 mm thick soft resin liner

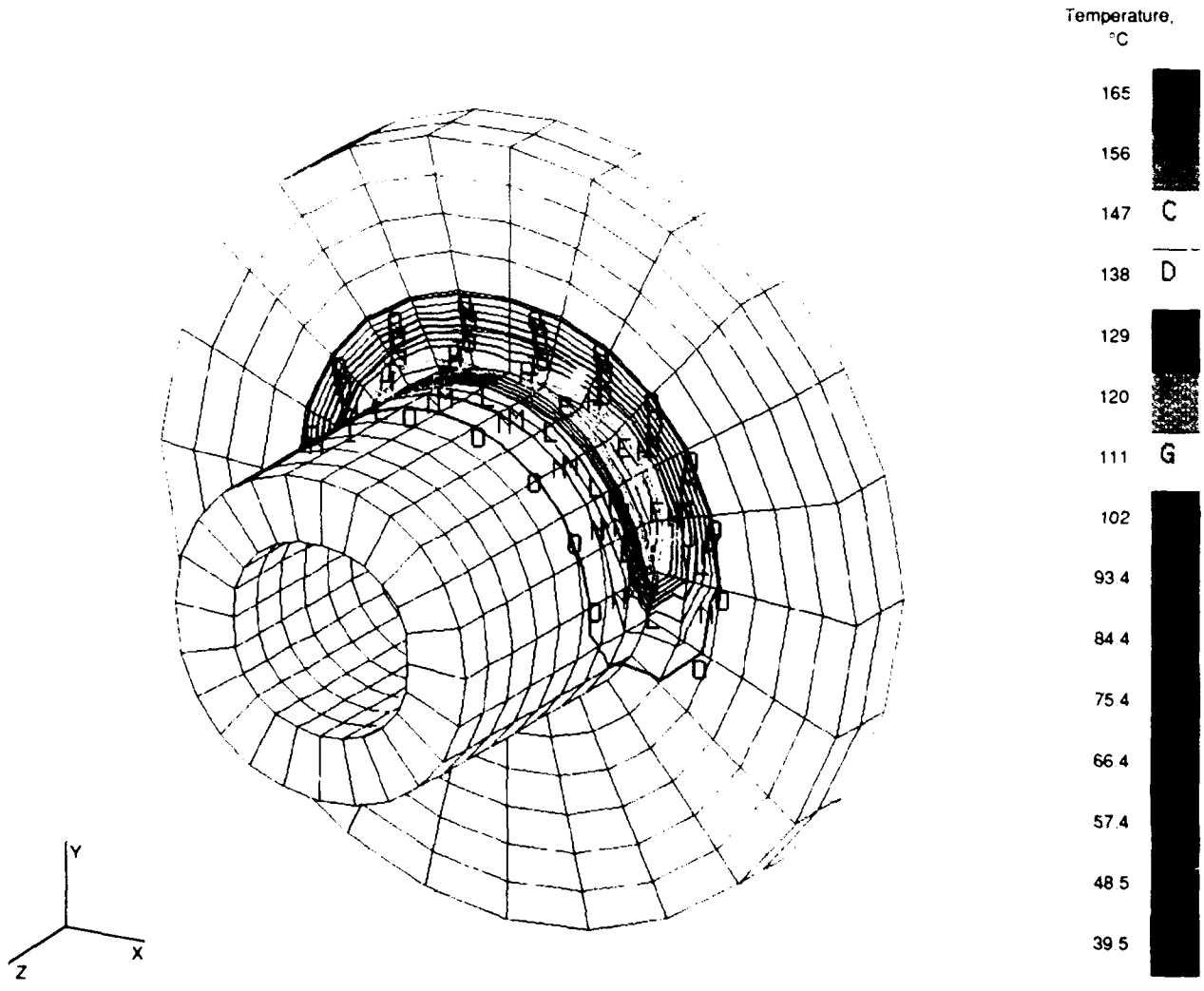

(a) Heat distribution function $q = q_m(2/\pi)(1 + \sin\theta)$.

Figure 3. – Tribosystem temperature contours for case I. Bearing has 6-mm-thick soft resin liner and various heat distribution functions.

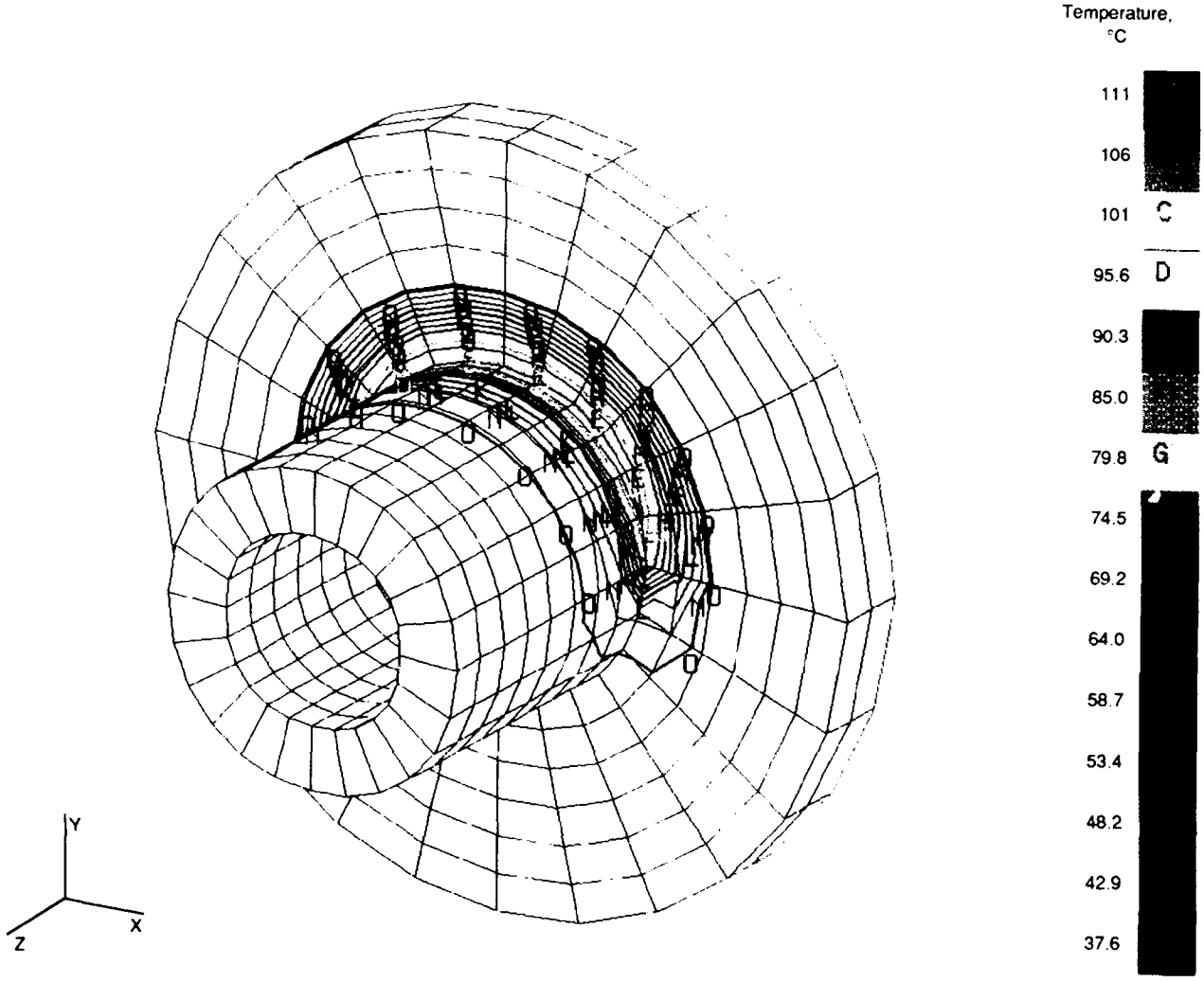

(b) Heat distribution function $q = q_m(2/\pi)$.

Figure 3.—Continued.

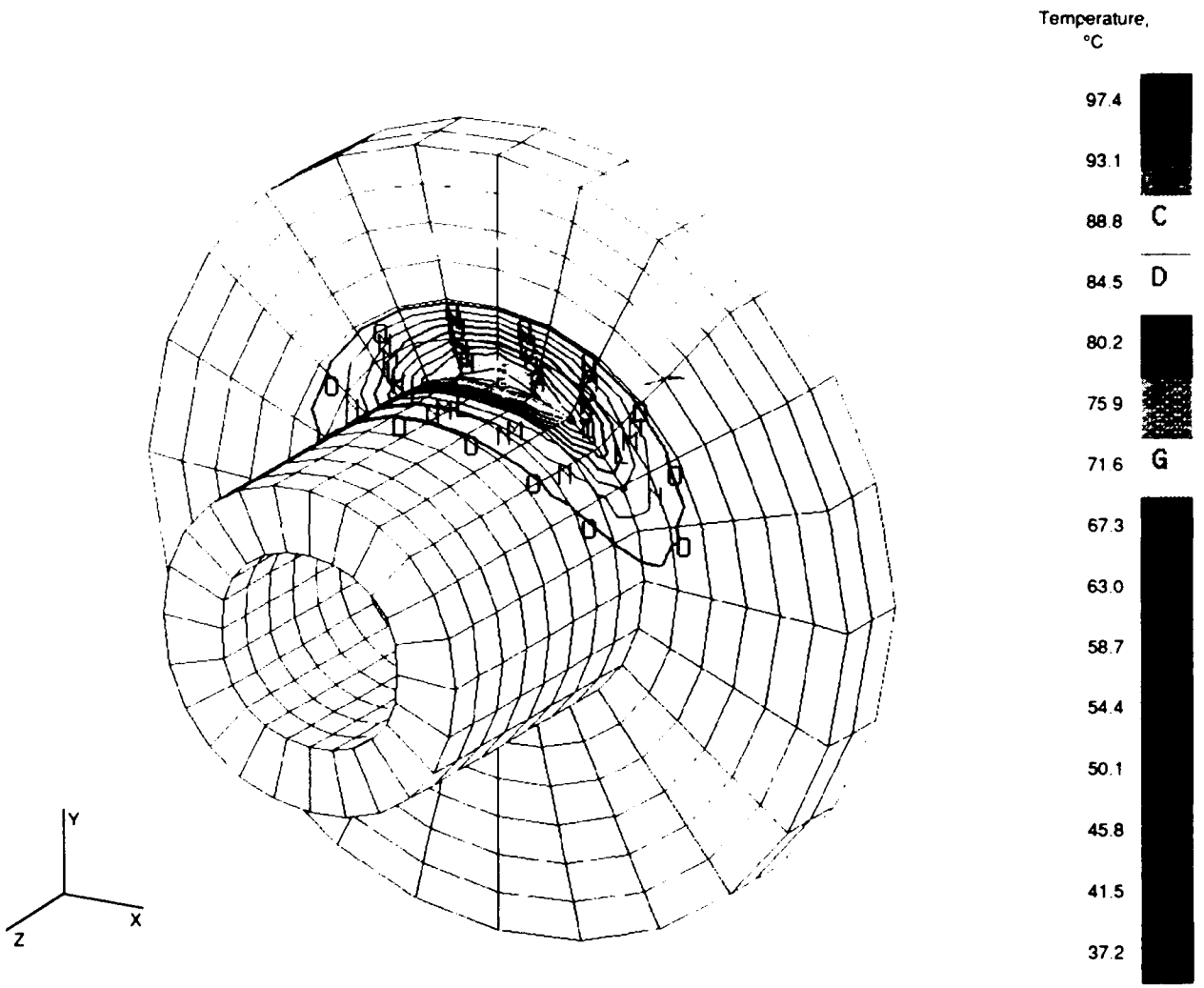

(c) Heat distribution function $q = q_m(2/\pi)(1-\sin\phi)$.

Figure 3.—Concluded.

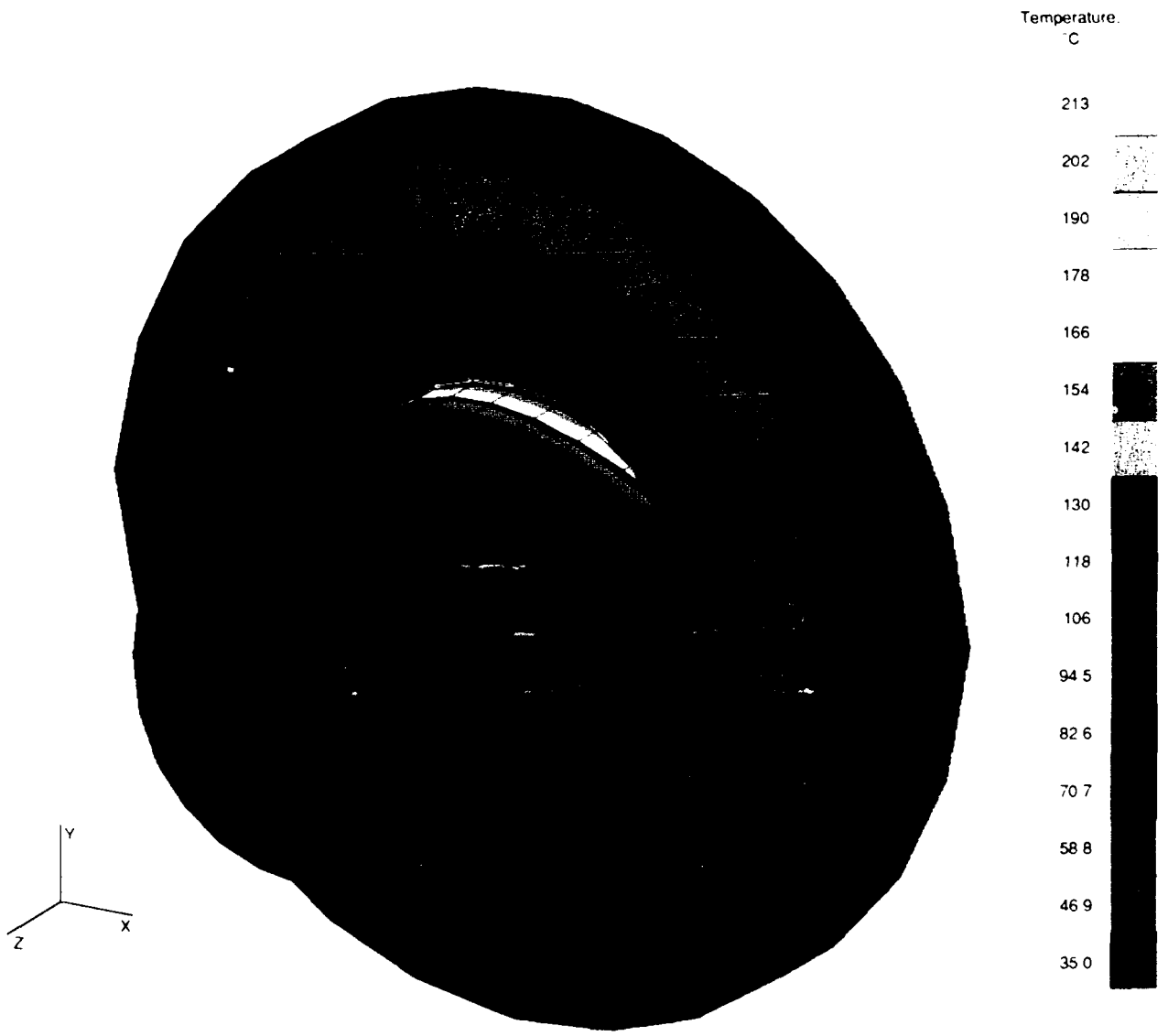

Figure 4 Tribosystem temperature contours for case II Bearing has 1 0 mm thick TiN coating

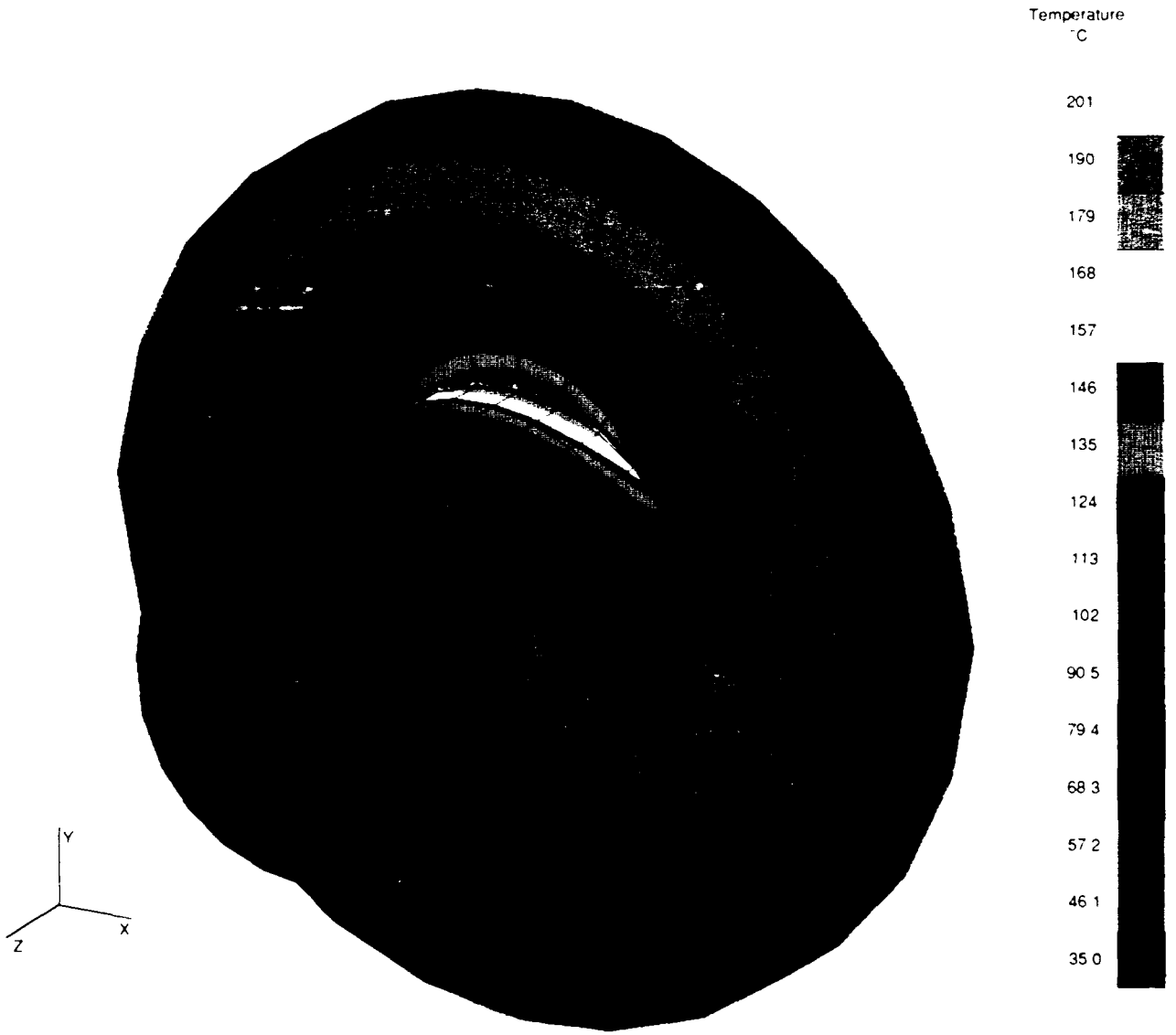

Figure 5.—Tribosystem temperature contours for case II. Bearing has 0.5 mm thick TiN coating.

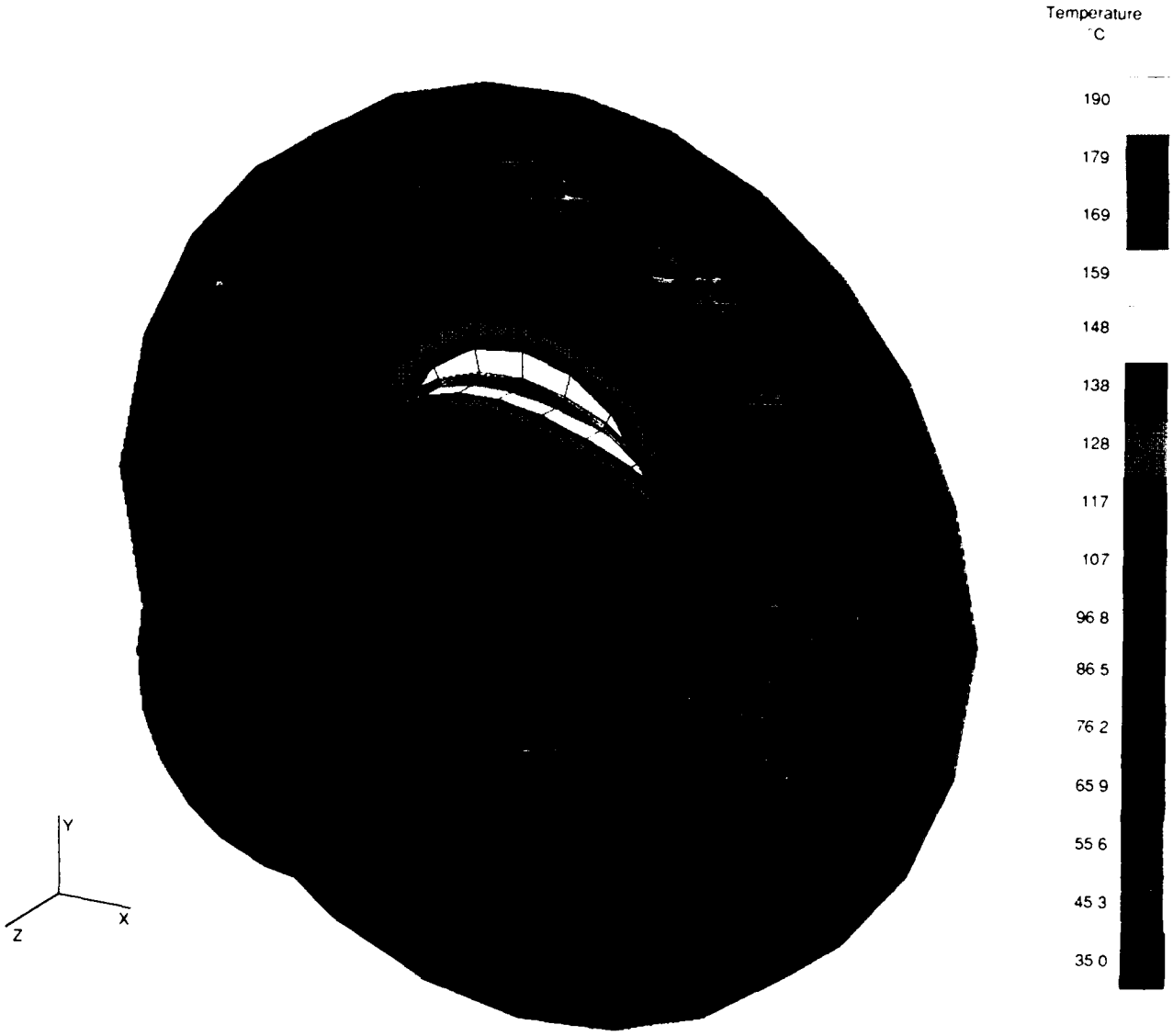

Figure 6. Tribosystem temperature contours for case II. Bearing has 0.125 mm thick TiN coating.

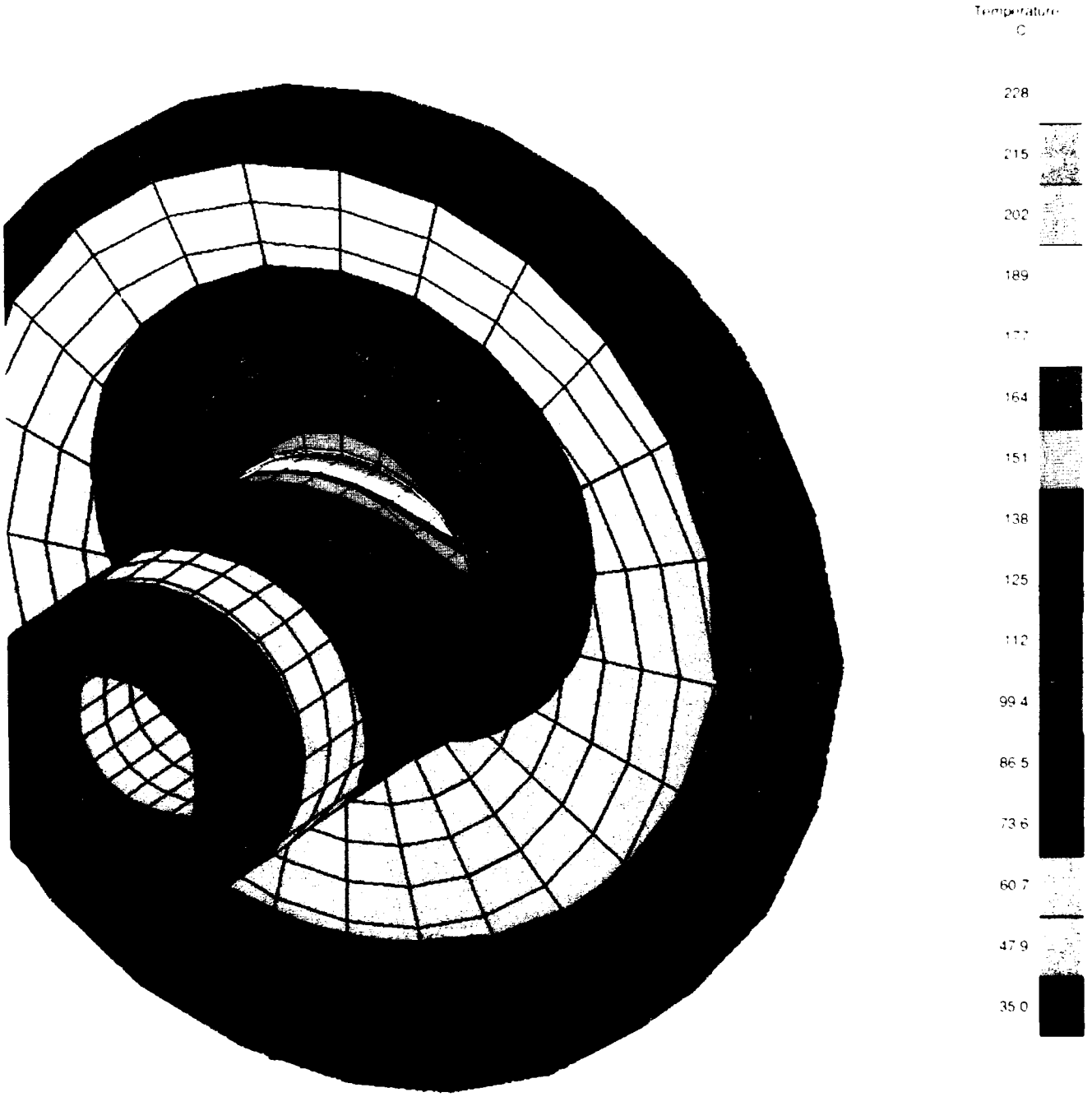

Figure [illegible] Driveshaft system temperature contours for case III. Bearing has 1.0 mm thick TiN coating; bearing outer radius = [illegible] cm

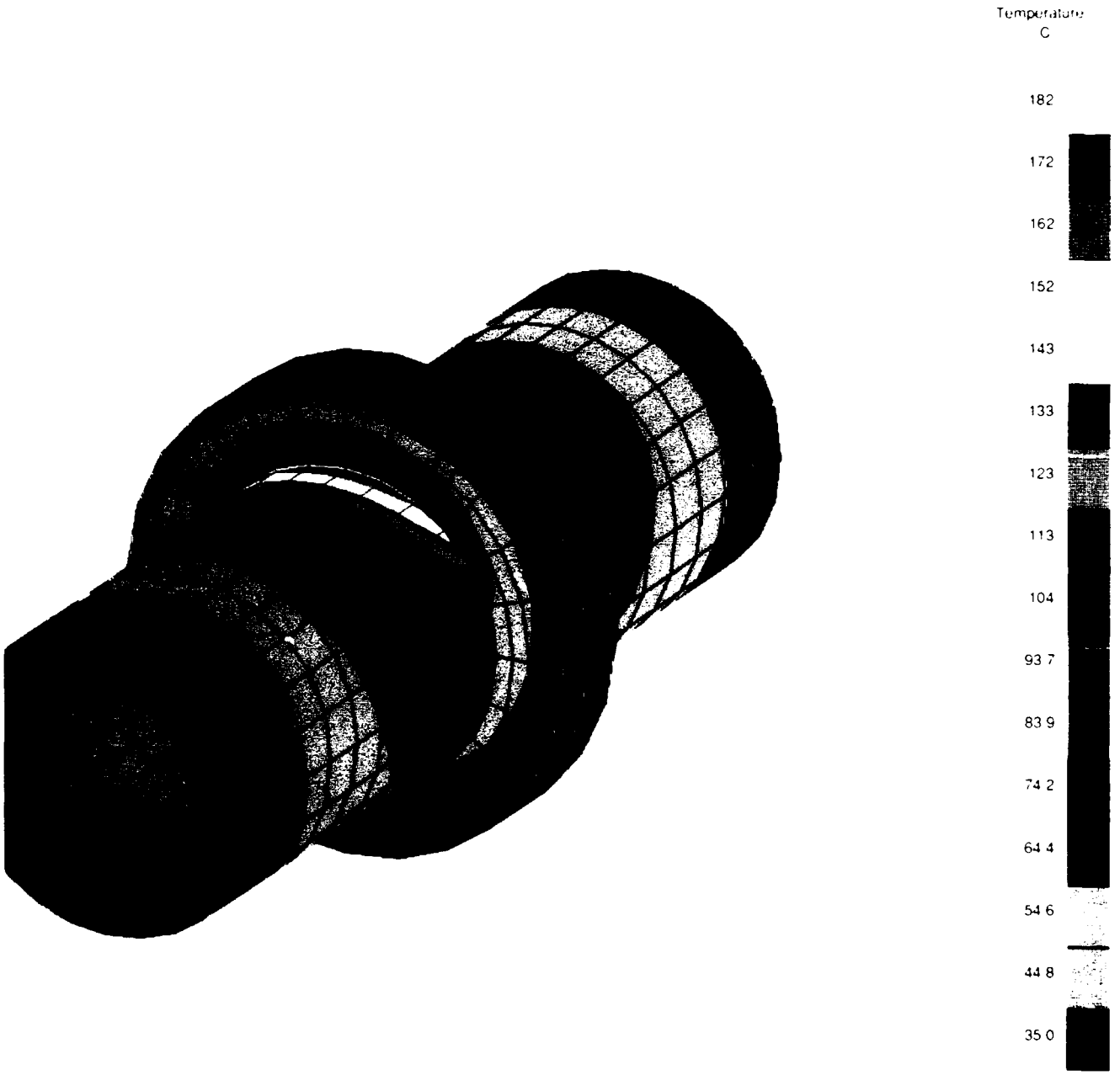

Figure 8. — Tribosystem temperature contours for case III. Bearing has 1.0 mm thick TiN coating, bearing outer radius = 3.8 cm.

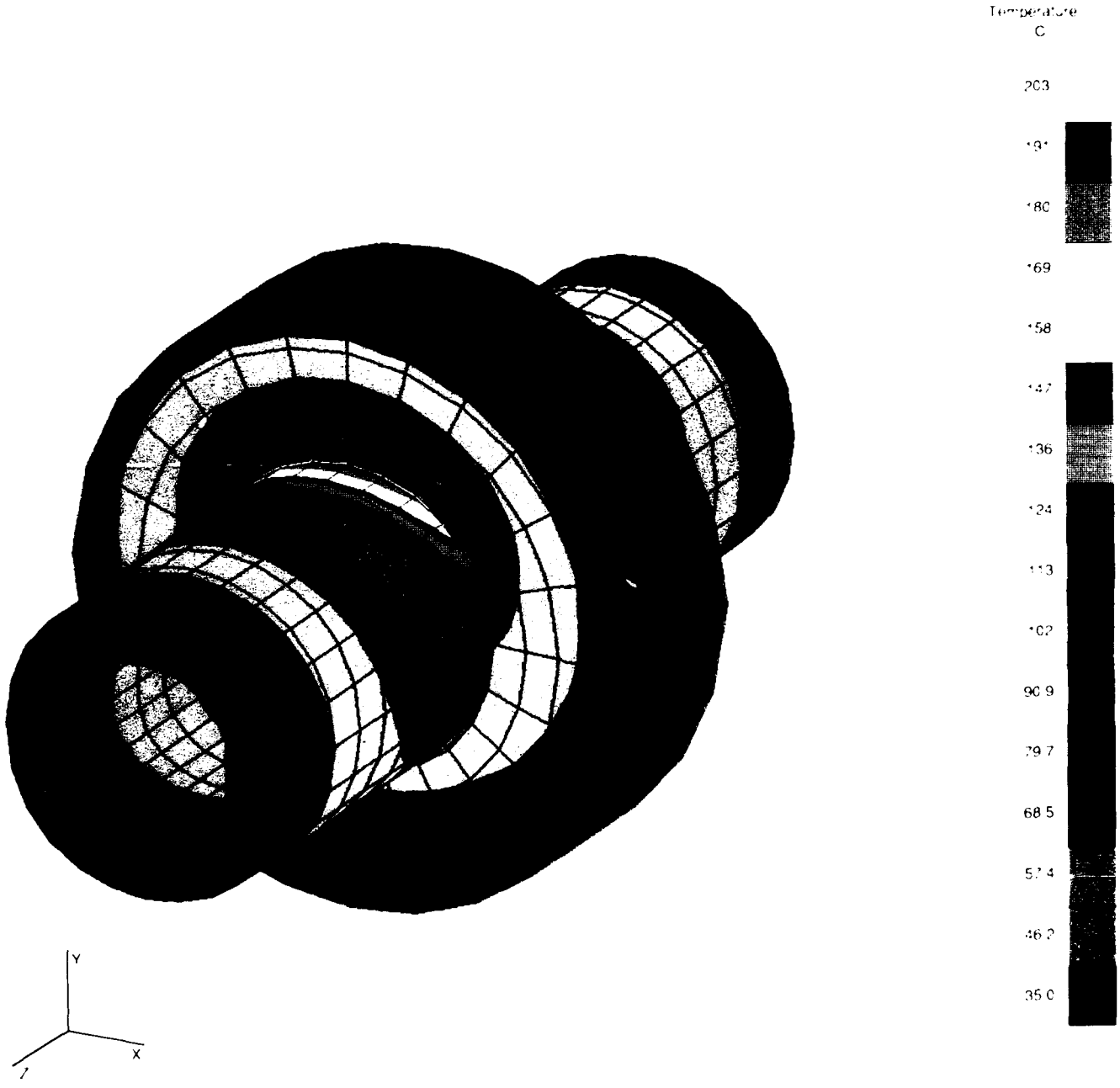

Figure 9. Turbosystem temperature contours for case III. Bearing has 1.0 mm thick TiN coating, bearing outer radius = 8.0 cm, bearing length = 3.2 cm.

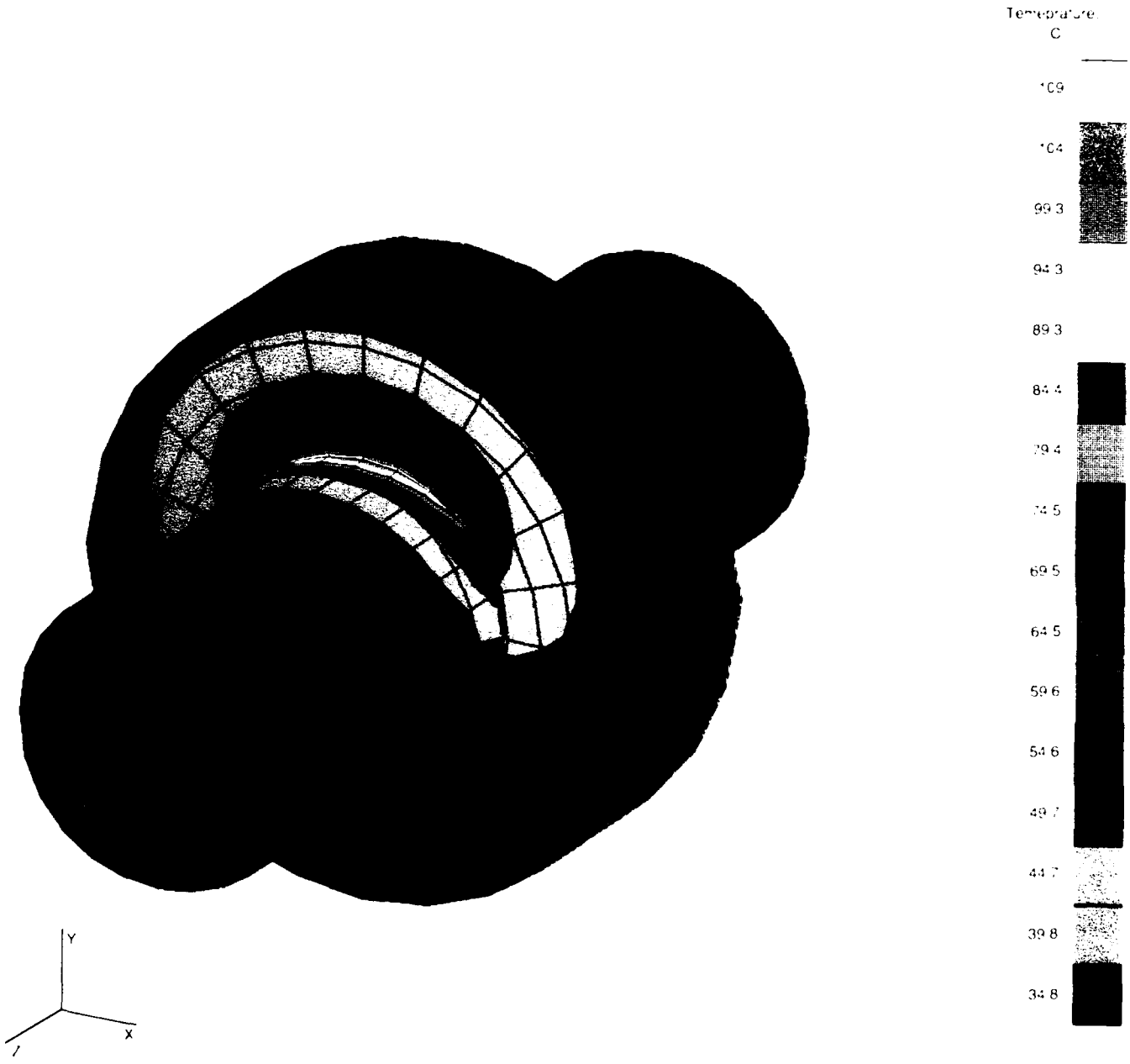

FIGURE 10.—Embossstem temperature contours for case III. Bearing has 1.0-mm-thick TiN coating and shaft outer surface coating. Heat-sink outer radius = 5 cm. Bearing length = 3.2 cm.

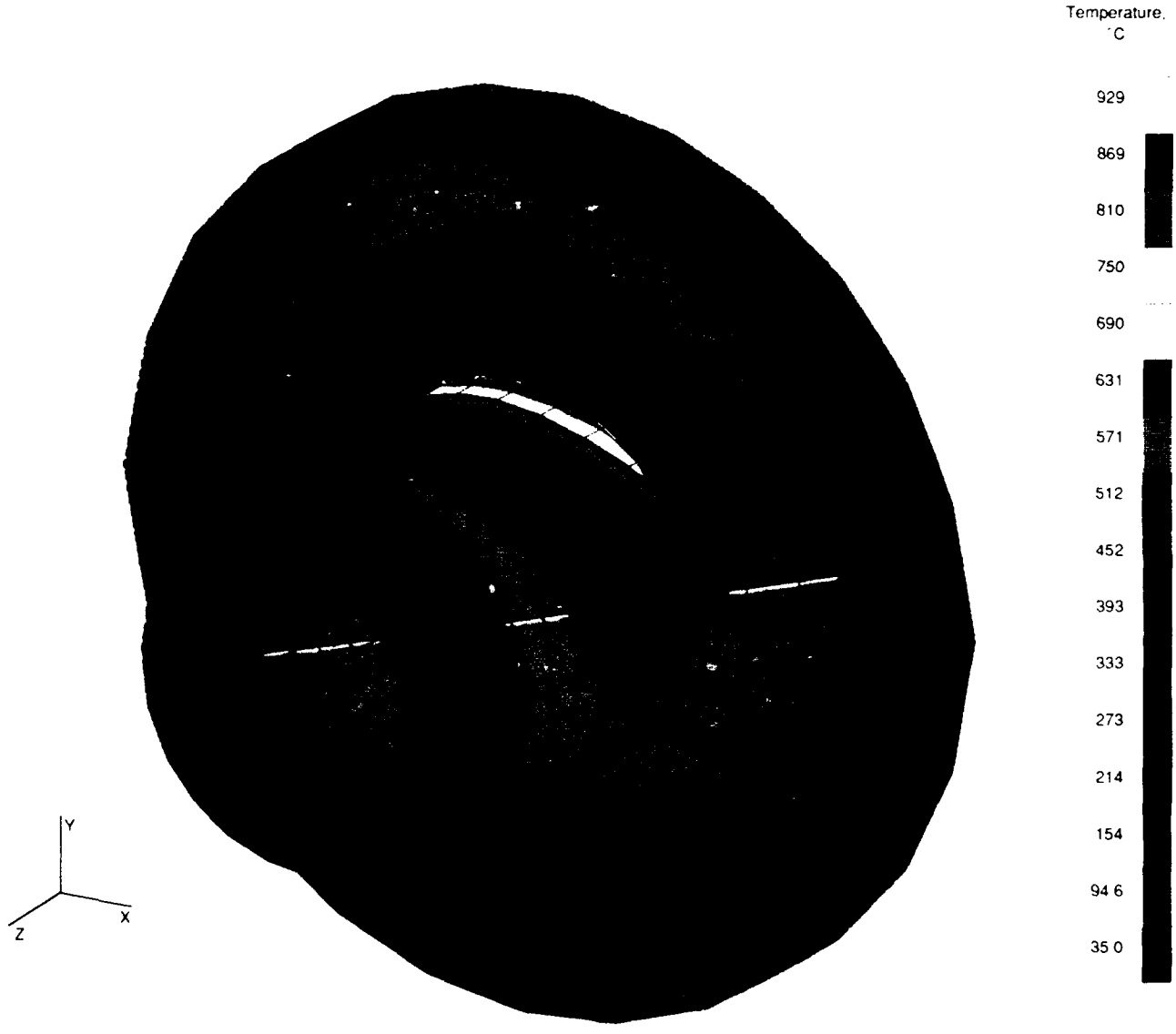

Figure 11.—Tribosystem temperature contours for case II. Bearing has 1.0 mm thick TiN coating. pV factor = 5362.5 N cm sec.

NASA
National Aeronautics and Space Administration

Report Documentation Page

1. Report No.	2. Government Accession No.	3. Recipient's Catalog No.
NASA TM-102513 AVSCOM TR 90-C-006		

4. Title and Subtitle

The Effect of Coatings and Liners on Heat Transfer in a Dry Shaft-Bush Tribosystem

5. Report Date

August 1990

6. Performing Organization Code

7. Author(s)

Mihir K. Ghosh and David E. Brewe

8. Performing Organization Report No.

E-5316

9. Performing Organization Name and Address

NASA Lewis Research Center
Cleveland, Ohio 44135-3191
and
Propulsion Directorate
U.S. Army Aviation Systems Command
Cleveland, Ohio 44135-3191

10. Work Unit No.

505-63-1A
1L161102AH45

11. Contract or Grant No.

12. Sponsoring Agency Name and Address

National Aeronautics and Space Administration
Washington, D.C. 20546-0001
and
U.S. Army Aviation Systems Command
St. Louis, Mo. 63120-1798

13. Type of Report and Period Covered

Technical Memorandum

14. Sponsoring Agency Code

15. Supplementary Notes

Mihir K. Ghosh, National Research Council—NASA Research Associate at Lewis Research Center, on leave from Mechanical Engineering Department, I.T.,B.H.U., Varnasi, 221005, India; David E. Brewe, Propulsion Directorate, U.S. Army Aviation Systems Command.

16. Abstract

The temperatures due to frictional heating within a solid lubricated or coated journal bearing were analyzed by using a finite element method. A solid model of the shaft-bush tribocontact was generated with an eight-node, three-dimensional, first-order isoparametric heat-transfer element and the Patran solid modeler software. The Patmar (Patran-Marc) translator was used to help develop the Marc-based finite element program for the system; this software was used on the Cray X-MP super computer to perform a finite element analysis of the contact. The analysis was performed for various liner materials, for thin, hard, wear-resistant coated bearings, and for different geometries and thermal cooling boundary conditions. The analyses indicated that thermal conductivity of the liner or coating material is the most vital thermal parameter that controls the interface temperature. In addition to design variations, the proximity of the cooling source to the heat-flux-generating interface is critically important to the temperature control in the system.

17. Key Words (Suggested by Author(s))	18. Distribution Statement
Heat transfer; Journal bearing coatings; High temperature; Dry lubrication; Finite elements; Thermal distribution; Frictional heat	Unclassified – Unlimited Subject Category 34

19. Security Classif. (of this report)	20. Security Classif. (of this page)	21. No. of pages	22. Price*
Unclassified	Unclassified	23	A03

NASA FORM 1626 OCT 86

*For sale by the National Technical Information Service, Springfield, Virginia 22161